Disassembly of Highly Excited Nuclei: From Evaporation to Vaporization

W. F. J. Müller[a], J.C. Adloff[c], M. Begemann-Blaich[a], P. Bouissou[e], J. Hubele[a], G. Imme[d], I. Iori[g], P. Kreutz[b], G.J. Kunde[a], S. Leray[e], V. Lindenstruth[a], Z. Liu[a], U. Lynen[a], R.J. Meijer[a], U. Milkau[a], A. Moroni[g], C. Ngô[e], C.A.. Ogilvie[a], J. Pochodzalla[b], G. Raciti[d], G. Rudolf[c], H. Sann[a], A. Schüttauf[b], W. Seidel[f], L. Stuttge[c], W. Trautmann[a] and A. Tucholski[b]

[a] Gesellschaft für Schwerionenforschung, Darmstadt, Germany
[b] Institut für Kernphysik, Universität Frankfurt, Frankfurt, Germany
[c] Centre de Recherches Nucléaires, Strasbourg, France
[d] Dipartmento di Fisica dell' Università, Catania, Italy
[e] Laboratoire National Saturne, CEN Sacly, Gif-sur-Yvette, France
[f] Forschungszentrum Rossendorf, Dresden, Germany
[g] Istituto di Scienze Fisiche, Università degli Sudi di Milano, Milano, Italy

Abstract

We have studied the fragmentation of Au projectiles interacting with targets of C, Al, Cu and Pb at an incident energy of E/A = 600 MeV. The experiment was performed with the ALADiN forward spectrometer at SIS. The employed inverse kinemantics allowed nearly complete detection of projectile fragments with charge $Z \geq 2$. In addition, the number of light particles for each collision was measured.

We compare different observables characterizing the event and investigate the impact parameter dependence of the fragmentation process.

It is found that the correlation between the mean multiplicity of intermediate mass fragments $\langle M_{imf} \rangle$ and Z_{bound}, the sum charges of all projectile fragments with $Z \geq 2$, is independent of the target nucleus. This universal behavior is consistent with an - at least partial - equilibration of the projectile fragment prior to its decay.

Finally we compare to two classes of statistical models, the sequential decay code GEMINI and statistical multifragmentation models.

Introduction

The decay mechanism of a nucleus with an excitation energy comparable to its total binding energy is one of the open questions in nuclear physics. The limiting cases are described in terms of evaporation and fission at low excitation energies, producing light particles and one or two heavy nuclear fragments, and complete vaporization at very high excitation energies, resulting in the total disassembly into mostly individual nucleons. Several theoretical scenarios have been proposed to describe the disassembly of a nucleus at intermediate excitation energies. They range from the near simultaneous breakup due to large fluctuations in regions of mechanical instability [1,2], to statistical multifragmentation models which calculate the available phase space for the decay of an expanded nuclear system [3,4], and sequential decay processes where equilibrium is re-established after each binary decay [5,6]. A prediction common to all models is the production of several intermediate mass fragments (IMFs). It is therefore obvious that the investigation of the experimental conditions leading to the formation of multiple IMFs must be the first step in the study of this process.

In this work we report on a semi-exclusive study of fragmentation of Au projectiles on lighter targets. The dependence of IMF production on impact parameter and other more direct experimental observables is investigated and compared to model calculations.

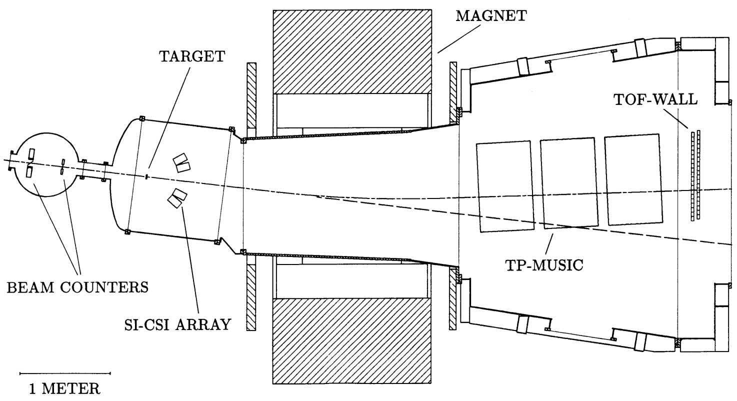

Fig. 1: Schematic view of the ALADIN facility. The dash-dotted line represents the trajectory of Au beam particles which were deflected by 8.2°.

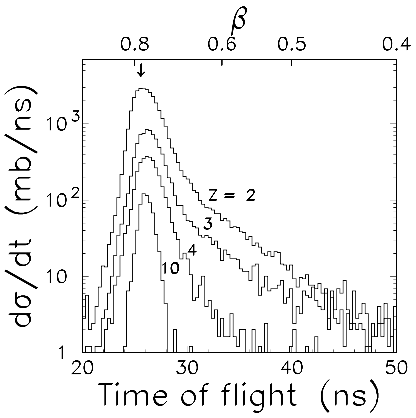

Fig. 2: Time of flight spectra for Z=2,3,4 and 10 fragments. The arrow indicates the beam velocity.

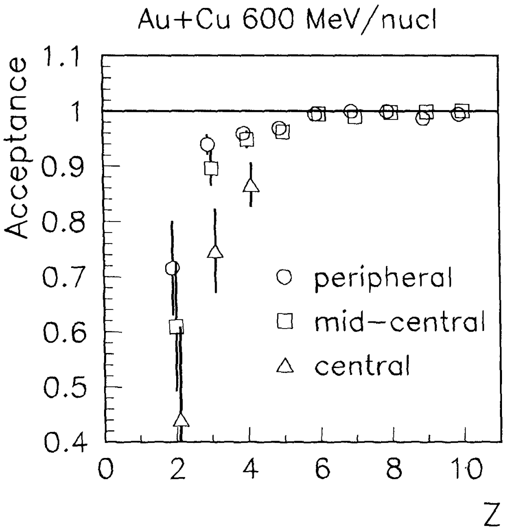

Fig. 3: Geometric acceptance of the TOF-Wall for the Cu target and three centrality cuts.

Experimental Details

The experiment was performed with the ALADIN forward spectrometer at GSI [7,8,9]. A schematic layout is shown in figure 1. The Au beam with an energy of E/A = 600 MeV was collided with targets of C, Al, Cu and Pb with a thickness of 200 to 500 mg/cm^2. The inverse kinematics focuses the fragmentation products of the Au projectiles into the forward direction. The charge and velocity of fragments with $Z \geq 2$ was determined with a time of flight wall positioned 6 m downstream of the target. The TOF wall covered an area of 1m x 1m with two layers of 40 scintillators each. This corresponds to an acceptance for beam velocity N=Z fragments of $\pm 4.7^o$ in the horizontal and $\pm 4.2^o$ in the vertical direction. Individual elements were resolved for $Z \leq 8$, for heavier elements a resolution of 2 charge units was obtained. Figure 2 shows the time of flight spectra of light fragments for the Cu target. We observe for all fragments with $Z \geq 2$ a peak centered at about beam velocity, only the distribution of fragments with $Z \leq 3$ has a tail towards lower velocities. The geometric acceptance for the beam velocity component is 75% or better except for Z=2 fragments produced in central interactions (figure 3). Fragments with $Z \geq 10$ were tracked and Z-identified in the TP-MUSIC detector positioned between the magnet and the TOF wall. This information was used to determine the emission angle of the fragments and to calibrate the charge response of the TOF wall for heavier elements.

Light particles, predominantly originating from the participant zone, were detected by a 64 element Si-CsI hodoscope covering the range $7^o \leq \theta_{lab} \leq 40^o$.

Experimental Results

With this almost complete coverage for beam rapidity fragments and the at least partial coverage for mid rapidity particles we can compare different methods of event characterization. We investigated three observables: M_{lp}, the multiplicity of light particles detected in the Si-CsI hodoscope, Z_{max}, the charge of the largest projectile fragment and Z_{bound}, the sum of all charges of projectile rapidity fragments with $Z \geq 2$. The quantity Z_{bound} was constructed to give the best estimate of the projectile spectator size. Fragments with Z=1 were excluded from Z_{bound} because their broad angular distribution leads to a low detection efficiency and makes the separation of participant and spectator contributions difficult. Figure 4 shows for Au+Cu collisions the correlation of the three observables M_{lp}, Z_{max} and Z_{bound}. In interactions leading to a large

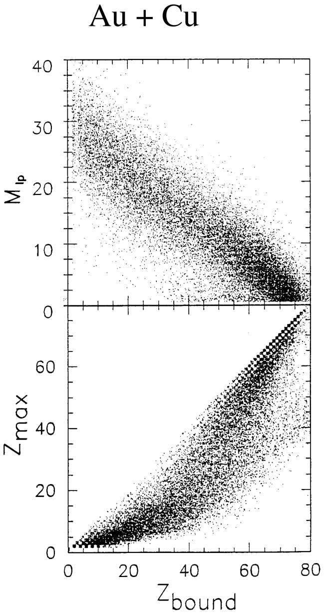

Fig. 4: Correlation of
M_{lp} Multiplicity of light particles in Si-CsI hodoscope.
Z_{max} Charge of the largest projectile fragment
Z_{bound} Sum of all charges of projectile rapidity fragments with $Z \geq 2$

for Au+Cu at E/A=600 MeV.

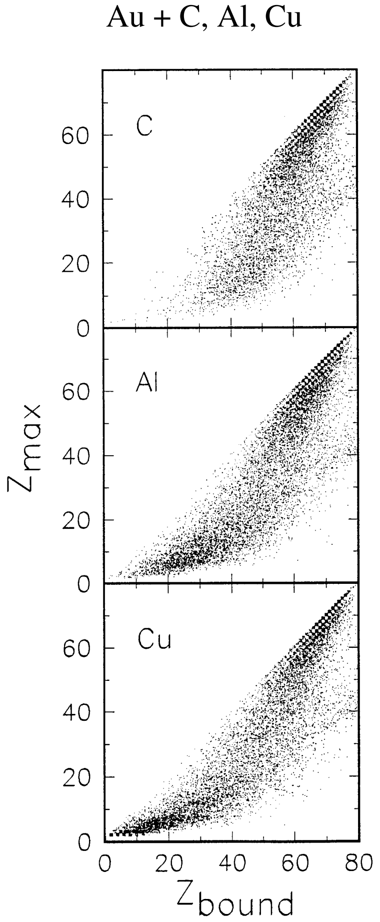

Fig. 5: Correlation of Z_{max} and Z_{bound} for the three reactions Au + C, Al and Cu.

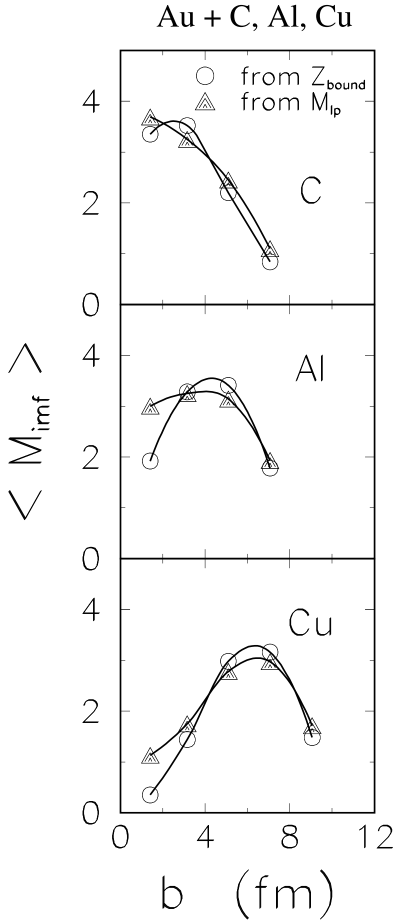

Fig. 6: Mean multiplicity of intermediate mass fragments $<M_{imf}>$ as a function of the reconstructed impact parameter.

Z_{bound} we observe only a few light particles as expected for peripheral collisions. With decreasing Z_{bound} the average light particle multiplicity $<M_{lp}>$ raises almost linearly indicating that both observables can be used for impact parameter selection. The correlation between Z_{max} and Z_{bound} is shown in the bottom part of figure 4. Z_{max} is by definition smaller than or equal to Z_{bound}. Events with Z_{bound} close to the projectile charge concentrate near the diagonal which corresponds to the detection of one heavy fragment and a small amount of charge in other complex fragments. For values of Z_{bound} around 50 one observes a rapid decrease of Z_{max}, most of the detected projectile spectator charge is not longer concentrated in one fragment. This transition from evaporation to breakup into multiple fragments can be observed at about the same value of Z_{bound} independent of the target as shown in figure 5.
For reactions on Cu and Al targets an appreciable fraction of the yield is located in the region where both Z_{bound} and Z_{max} are small. In these most violent events either a very light spectator is formed or the spectator has an excitation energy that will lead to complete disassembly into mostly nucleons and a few complex fragments. For reactions on the C target, however, the cross section decreases rapidly for Z_{bound} below 30 indicating that there is not enough energy available for the total disassembly of the spectator. A small fission contribution can be clearly identified in the region $Z_{max} \sim 40$ and $Z_{bound} \geq 70$.

This evolution from evaporation in the most gentle collisions via multifragment production to vaporization in the most violent collisions suggests a corresponding rise and fall of the production of intermetiate mass fragments (IMFs) as a function of the impact parameter. We define an IMF as a fragment with $3 \geq Z \geq 30$. To determine the impact parameter b from the observables M_{lp} and Z_{bound}, we adopted a geometric cross section method first used in [10]. Using a sharp cutoff picture we calculated the maximum impact parameter accepted by our trigger condition from the observed reaction cross section. Bins in M_{lp} or in Z_{bound} are then successively associated with impact parameter bins that represent the same cross section. Figure 6 shows the mean multiplicity of intermediate mass fragments $<M_{imf}>$ as a function of the impact parameter scales reconstructed from M_{lp} and Z_{bound}. For the C target, the mean IMF multiplicity increases with decreasing impact parameter and reaches a value of 3-4 for the most central collisions. Interactions with Al are similar, but show the onset of a decrease of $\langle M_{imf} \rangle$ for $b \leq 4$ fm. For the Cu target the maximum $\langle M_{imf} \rangle$ is again 3-4 and is found at an even larger impact parameter of 6-7 fm. The largest multiplicity of IMFs is therefore observed in different reaction geometries, in Au + C interactions in central collisions with full overlap of projectile and target and in Au + Cu reactions in semi-central collisions with only partial overlap. It is interesting to note that, within the participant-spectator model [11] the size of the projectile spectator for impact parameters corresponding to the maximum IMF multiplicity is about 150 nucleons for all three targets. The two impact parameter scales agree remarkably well. The small deviations can be interpreted as the influence of autocorrelations between $\langle M_{imf} \rangle$ and Z_{bound}, resulting in a sharper decrease of $\langle M_{imf} \rangle$ towards small b on the Z_{bound} derived scale, and the larger fluctuations of M_{lp}, resulting in a flatter distribution for the M_{lp} derived scale [9].

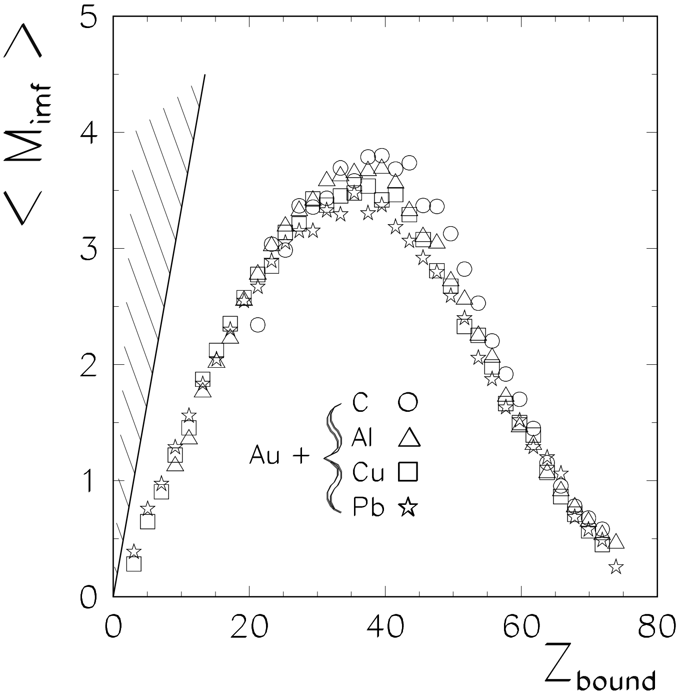

Fig 7: Correlation between mean IMF multiplicity and Z_{bound} for Au + C, Al, Cu and Pb reactions at E/A = 600 MeV. The shaded region is excluded by our definition of an IMF and Z_{bound}.

In contrast to the clear target dependence of the relation between $\langle M_{imf} \rangle$ and impact parameter we observe an almost universal correlation between $\langle M_{imf} \rangle$ and Z_{bound} as illustrated in figure 7 for the reactions Au + C, Al, Cu and Pb. A maximum mean IMF multiplicity of 3-4 is reached near $Z_{bound} = 40$ with only a weak systematic trend towards smaller peak values for heavier targets.

The universal correlation of $\langle M_{imf} \rangle$ and Z_{bound} for all targets despite the different collision geometries for maximum IMF production is compatible with the formation of a chemical equilibrium during the fragmentation process. To test whether also an - at least partial - dynamical equilibrium is formed we have examined the velocity distribution of the fragments. Figure 8 shows the ratio of the rms-width of the transverse and longitudinal velocity as a function of the fragment charge for three cuts in Z_{bound}. The ratio of 1 ± 0.2 indicates an almost isotropic velocity distribution.

Comparison with Statistical Models

Our experimental results are consistent with a simple two-step model. In a first, fast collision stage a prefragment is formed with mass $A_1 = A_{proj} - \Delta A$ with ΔA the number of nucleons ejected from the projectile. This prefragment then decays in a second stage. The abrasion model predicts a linear relationship $\langle E^* \rangle = \varepsilon_1 * \Delta A$ between the average excitation energy $\langle E^* \rangle$ and ΔA with an excitation energy per removed nucleon of $\varepsilon_1 = 13$ MeV [12]. Cascade models predict substantially higher values, e.g. $\varepsilon_1 = 28$ MeV in a recent work with the ISABEL code [13]. In a more detailed calculation with the Boltzmann - Uehling - Uhlenbeck (BUU) model [14] we find a dependence of ε_1 on the number of removed nucleons ΔA. The value of ε_1 raises from 12 MeV in central Au+Cu collisions leading to a prefragment with A_1~100 to about 28 MeV in the most peripheral collisions with ΔA ~ 10 [8].

A variety of statistical models has been proposed to describe the decay of an excited prefragment. We have compared the predictions of the evaporation code GEMINI [6], which describes the sequential decay of a system at normal density and the statistical multifragmentation models of Bondorf et al. (Kopenhagen SMF) [4] and Gross et al. (Berlin SMF) [3], which describe the simultaneous decay of an expanded nuclear system, with our data. Using the BUU estimates for the distribution of the prefragment size A_1 and the average excitation energy $\langle E^* \rangle$ as input we have calculated for all three models the resulting correlation be-

Fig 8: The mean longitudinal velocity (upper part) and the ratio of the transverse and longitudinal rms velocity (lower part) as a function of the fragment charge. The different symbols correspond to different cuts on Z_{bound}. The dotted line in the upper part marks the beam velocity. The threshold of the MUSIC detector restricts this analysis to fragments with charge $Z \geq 8$.

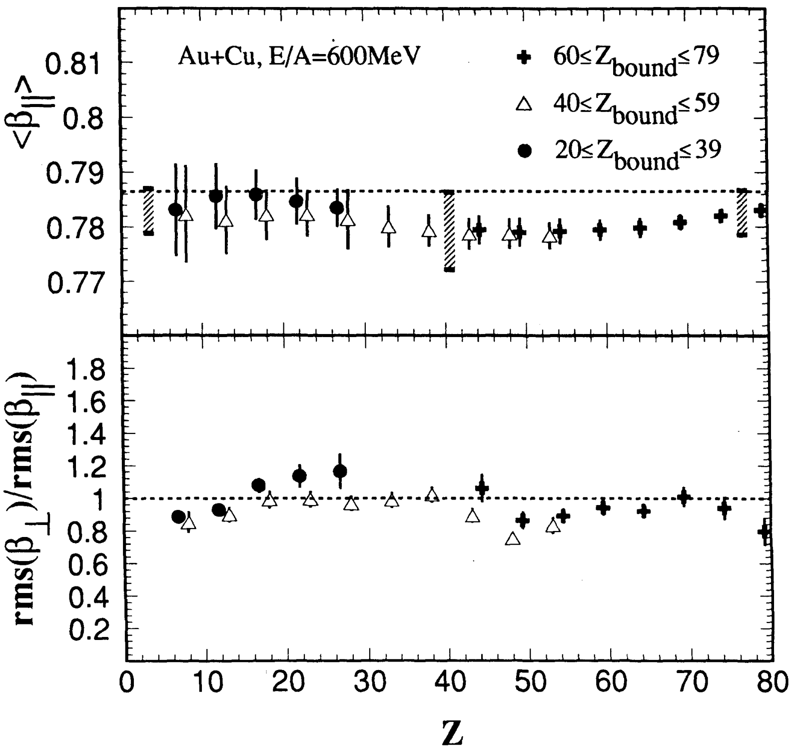

Fig 9: Comparison of the $\langle M_{imf} \rangle$ - Z_{bound} correlation for Au + Cu reactions (squares) with predictions of the sequential decay code GEMINI (left part) and the statistical multifragmentation models of Gross and co-workers (center part) and of Bondorf and co-workers (right part). The lines represent excitation functions for different initial systems (A_1,Z_1) = (100,40), (131,54) and (190,75). The shaded bands are predictions based on initial conditions provided by BUU simulations.

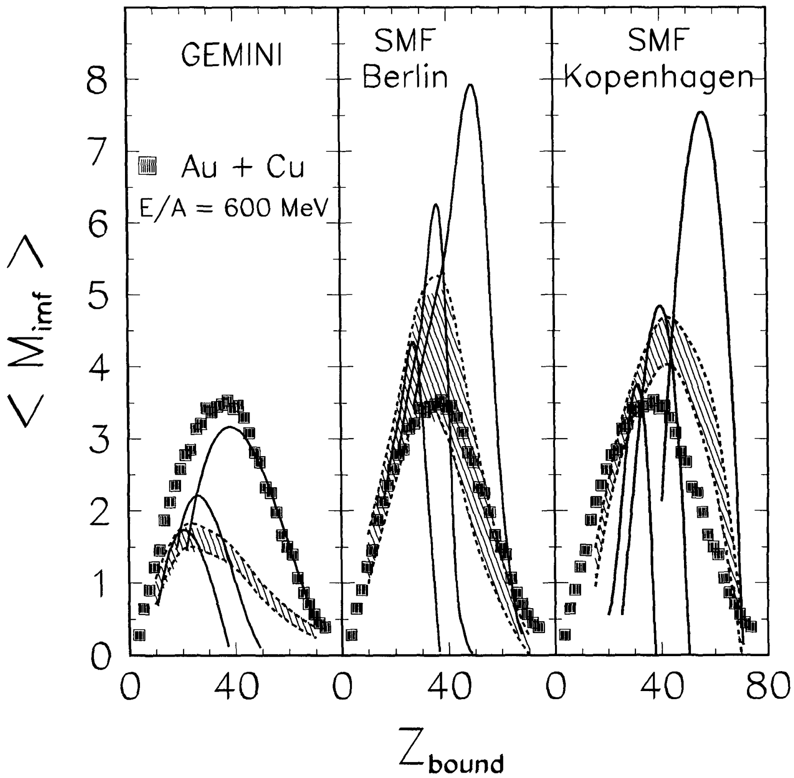

tween $\langle M_{imf} \rangle$ and Z_{bound} [15]. Figure 9 summarizes the comparison between Au+Cu data (squares) and the BUU plus statistical model calculations (shaded bands). The width of the bands reflects the variation of the BUU estimates for A_1 and $\langle E^* \rangle$ for the four different targets. The lines represent excitation functions for three prefragment sizes (A_1,Z_1) = (100,40), (131,54) and (190,75). The GEMINI calculation clearly underestimates the IMF multiplicity by about a factor of 2. The Kopenhagen model slightly overestimates the peak $\langle M_{imf} \rangle$ value and predicts a too rapid decrease of $\langle M_{imf} \rangle$ at small Z_{bound} values. The best overall agreement with our experimental observations is achieved with the Berlin model.

Summary and Conclusion

We have studied the fragmentation of Au projectiles interacting with targets of C, Al, Cu and Pb at an incident energy of E/A = 600 MeV. It was found that for Au+C interactions the largest number of IMFs is

produced in central collisions. For heavier targets the maximum of the mean IMF multiplicity occurs for more peripheral interactions. The maximum is 3-4 IMFs for all targets. We found an universal correlation of $<M_{imf}>$ and Z_{bound}. This target independence suggests that a chemical equilibrium is being established during the fragmentation process.
Hybrid models, employing a BUU calculation to determine the prefragment size and excitation energy and a statistical multifragmentation model to describe the subsequent decay reproduce the observed $<M_{imf}>$ - Z_{bound} correlation. A calculation based on the sequential decay code GEMINI clearly underestimates the IMF production.

The models discussed in this work either neglect the fluctuations generated during the collision and any dynamics during the fragmentation process or, as in the QMD model, take all this into account but lack a treatment of statistical decays. Having now determined a set of optimal conditions for the multifragment decay of a large system, we will focus in the next experimental step on a detailed investigation of momentum space observables. It will be interesting to confront these experiments with more detailed models which describe the collision and fragmentation dynamics as well as statistical decays.

References

[1] G. Bertsch and P.J. Siemens, Phys. Lett. **126B**, 9 (1983)
[2] C.J. Pethick and D.G. Ravenhall, Nucl. Phys. **A471**, 19c (1987)
[3] D.H.E. Gross and H. Massmann, Nucl. Phys. **A471**, 339c (1987)
[4] H.W. Barz *et al.*, Phys. Lett **169B**, 318 (1986)
[5] W.A. Friedman and W.G. Lynch, Phys. Rev. C **28**, 16 (1983)
[6] R.J. Charity *et al.*, Nucl. Phys. **A483**, 371 (1988)
[7] The ALADIN collaboration, GSI-Nachrichten 02-89 (1988)
[8] C. Ogilvie *et al.,*Phys. Rev. Lett. **67,** 1214 (1991)
[9] J. Hubele *et al.*, Z. Phys. **A 340**, 263 (1991)
[10] W.U. Schröder *et al.*, Phys. Rep. **45**, 301 (1978)
[11] J. Gosset *et al.*, Phys. Rev. C **16**, 629 (1977)
[12] J.-J. Gaimard and K.-H. Schmidt, Nucl. Phys. **A531**, 709(1991)
[13] K. Sümmerer, private communication
[14] W. Bauer, private communication
[15] J. Hubele, Phys. Rev. C **46**, in press